Digest Journal of Nanomaterials and Biostructures Vol. 11, No. 3, July - September 2016, p. 741 - 752

EFFECT OF VARIATION OF Mn/Zn CONTENT ON THE STRUCTURAL, ELECTRICAL AND MAGNETIC PROPERTIES OF Mn-Zn FERRITE

A. HAKEEM[a], I. AHMAD[b], G. MURTAZA[b, c*], G. MUSTAFA[b], M.KANWAL[b], M. T. FARID[b], M. HUSSAIN[b], H. R. LODHI[b] , M. AHMAD[d]
[a]*Department of Physics, Govt. Post Graduate college Jampur, Pakistan.*
[b]*Department of Physics, Bahauddin Zakariya University, Multan,60800 Pakistan.*
[c]*Department of Physics, GC University Faisalabad, Layyah Campus, Layyah 31200, Pakistan.*
[d]*Department of Physics, COMSATS Institute of Information Technology, Lahore 54000, Pakistan.*

Nano sized Mn-Zn ferrite particles were synthesized by co-precipitation method. The X-ray diffraction analysis of sintered powder at 1000°C reveals the ferrite possesses spinel face centered cubic structure. Particle size is observed by SEM ranging from 50nm to 85nm. The magnetic properties are measured by using the Physical property measurements (PPMS) technique. The Fourier transform infrared spectroscopy is used to detect the presence of the metallic compounds in the ferrite sample. Lattice constant is proportional to the Mn contents and it decreases with the increase of Zn contents. The actual density of the ferrites was found to be increasing, where as X-ray density depend on the molecular weight. Lattice constant of the material tends to decrease with an increase of Mn contents.

(Received April 20, 2016; Accepted July 18, 2016)

Keywords: Fourier transform infrared (FTIR) spectroscopy; Scanning Electron Microscopy (SEM); X-ray diffraction; Physjcal Property Measurements (PPMS)

1. Introduction

Manganese-Zinc (Mn-Zn) elements are important in many high frequency power electronics and magnetic applications as a consequence of their high magnetic permeability and electrical resistivity. The concentration of ferrous and ferric ions and their distribution between the tetrahedral and the octahedral sub-lattices, play a critical role in determining their magnetic and electrical properties [1]. Zinc ferrite has long been the subject of studying among the spinel ferrites, because it possesses unique properties such as chemical and thermal stability and the magnetic properties depends mostly on particle size [5]. Soft magnetic ferrites are used as cores in modern electronic components such as recording heads, filters, switching power supply transformers, amplifiers, etc. Mn-Zn ferrites attracted much attention due to a wide range of relative magnetic permeability value (from 10^3 to 10^4) and low magnetic losses as well as increased thermal stability, high saturation magnetic flux density at high temperatures (Bs>0.4T at 370K) and a relatively high curie temperature, operating frequency is usually in the range of 1 KHz to 1MHz but in some applications the frequency is in GHz range [6, 7]. Furthermore, excellent corrosion resistance and chemical stability enable them to be applied in extreme conditions.

Recently, a variety of preparation routes have been examined for Mn-Zn ferrite production; mechano-chemical processing [8, 9], Chemical co-precipitation method [10], sol-gel [11], or micro emulsion [12]. This paper deals with Mn-Zn ferrites prepared by co-precipitation technique. The spinel ferrites (MFe_2O_4, where M= Mn, Ni, Co,Zn, Cd, etc) are particularly important magnetic material due to their use in electromagnetic interference (EMI) in the MHz range like TV ghost suppressor [13-16]. Mn-Zn ferrites having spinel structure with Fe ions at

*Corresponding author:mrkhichi@gmail.com

both tetrahedral (A-site) and octahedral (B-site) while Mn^{2+} and Zn^{2+} ions occupy tetrahedral (A-site). The introduction of different metal cations concentration into the soft ferrites, leads to change in electric and magnetic properties of the material considerably [17]. Requirements for magnetic cores used in switching power supply transformers include soft magnetism, easy magnetization with a small external magnetic field, and low loss. Magnetic materials are classified into two groups, metallic materials and oxide materials. The electric resistance of the metallic materials is generally lower; driving the transformer of a switching power supply causes large eddy current loss at high frequencies. In order to suppress loss Mn-Zn ferrites are used in the transformer rather than metallic materials. Mn-Zn ferrites are very important in biomedicine, as magnetic carriers for biodegradation enzymes and protein immobilization [18]. The drawback of Mn-Zn ferrites is their saturation magnetic flux density which is lower than those in metallic soft materials. This means that a larger volume of ferrite core is required to produce the same amount of magnetic flux as metallic cores produce. In the present paper, we have synthesized the Mn-Zn ferrite by co-precipitation technique to study the variation effect of Mn/Zn contents on the structural, electrical and magnetic properties of Mn-Zn ferrite.

2. Experimental method and calculations

2.1 Materials

All the chemical re agents $Zn(NO_3)_2.6H_2O$, $Mn(NO_3)_2.6H_2O$ and anhydrous ferric nitrate $Fe(No_3)_3.9H_2O$ of Sigma Aldrich are taken.

2.2 Synthesis method

Nano crystalline ferrites Mn-Zn are prepared by co-precipitation method. The desired composition is obtained by taking stoichiometric amount of Zn $(NO_3)_2.6H_2O$, Mn $(NO_3)_2.6H_2O$ and Fe $(No_3)_3.9H_2O$ are dissolved in deionized water. On adding the ammonia solution the pH of the solution becomes10 and it becomes neutral after stirring 2hrs. Put the solution in a sonicater for 20 minutes then place it for a while in the ultrasonic bath so that precipitate will settle down then filter it with a filter paper. Wash the precipitate with deionized water until it becomes free of impurities. The product is dried to remove water contents. The dried powder is sintered at 1000ºC for five hours.

2.3 Characterization

The X-ray diffraction (XRD) patterns of the samples are recorded on a BRUKER X-ray powder diffractometer using CuKα (1.54060Å) radiation. The scans of the selected diffraction peaks are carried out in the step mode. The crystallite size was calculated by the help of a Scherrer's formula [19].

2.4 Calculations

The lattice constant 'a' can be obtained by using the following relation:

$$a = d_{hkl}\sqrt{h^2 + k^2 + l^2} \qquad (1)$$

where d_{hkl} is the distance between the adjacent Millar planes (h k l). It can be calculated by the relation:

$$d_{hkl} = \frac{n\lambda}{2\sin\theta} \qquad (2)$$

with n = 1 for the cubic system, XRD data can be used to calculate the X-ray density ρ_x which is given by Smit and Wijin [20].

$$\rho_x = \frac{ZM}{Na^3} \qquad (3)$$

Where M is the molecular weight and N is the Avogadro's number (6.023 x10^{23}atoms/mol), Z is the number of molecules pet unit cell (for oxide compounds having cubic spinel structure Z = 8) and 'a' is the lattice parameter in (cm). The average particle size is determined by using the Scherrer's relation

$$D = \frac{0.9\,\lambda}{\beta cos\theta} \qquad (4)$$

Where D is crystallite size, θ is the Bragg's angle, λ is the wavelength of the X-ray radiation, and β is the line width at maximum height [21].

The X-ray diffraction of calcinated Mn-Zn ferrite sample sintered at 1000ºC are subject to calculate the average particle size using Debye – Scherrer formula. The crystalline structure of composite Nano particles is characterized by Scanning Electron Microscope (SEM).The two theta value of the (311) plane, full width half maximum value of the (311) plane calculated using a scientific peak fit software and calculated particle size using the measured FWHM values. It is well known that high calcinations temperatures increase particle size. This increase is not desired since the main advantage of co-precipitation method in relation to ceramic one is to obtain fine particles with a narrow size distribution in low calcinations temperatures. Thus, the best way to produce Mn-Zn ferrite to single phase is to increase the calcinations time.

3. Results and discussions

The x-ray diffraction measurement of ferrite fired at 1000°C shows that all peaks of Mn-Zn ferrite consist with those of a typical spinel face centered cubic structure. Fig. 2 illustrates the XRD patterns of the ferrite. The XRD pattern of the ferrite indicates that the material is based on cubic spinel structure. The average crystallite size is in the range of 50-85nm. The strong diffraction peaks at 2θ = 17.73°, 30.22°, 35.53°, 43.30°, 53.58°, 57.35°, 62.72°,72.95° corresponds to (220), (311), (400), (422), (511), (440), (533), (444) typical planes of Mn-Zn ferrite spinel structure according to the JCPDS (Joint Committee on powder Diffraction Standards) cards [22].There are some secondary peaks at 2θ = 22°, 31°, 47°, 52° indicated by asterisk, these may be due to the excess quantity of ZnO. The Scanning Electron Microscope (SEM) images are shown in Fig. 1.

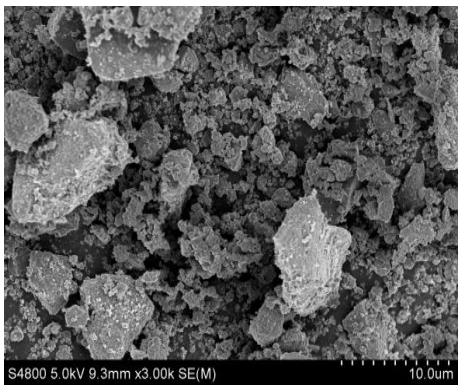

$Mn_{0.2}Zn_{0.8}Fe_2O_4$

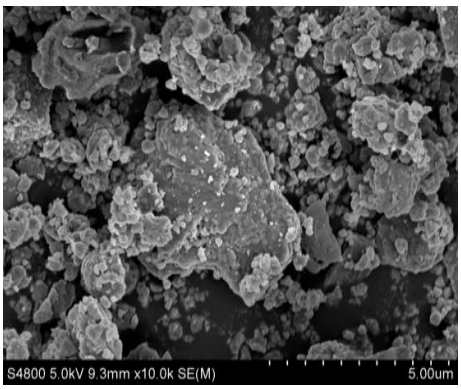

$Mn_{0.8}Zn_{0.2}Fe_2O_4$

Fig. 1 Scanning Electron Microscope (SEM) images of (a) $Mn_{0.2}Zn_{0.8}Fe_2O_4$, (b) $Mn_{0.8}Zn_{0.2}Fe_2O_4$,

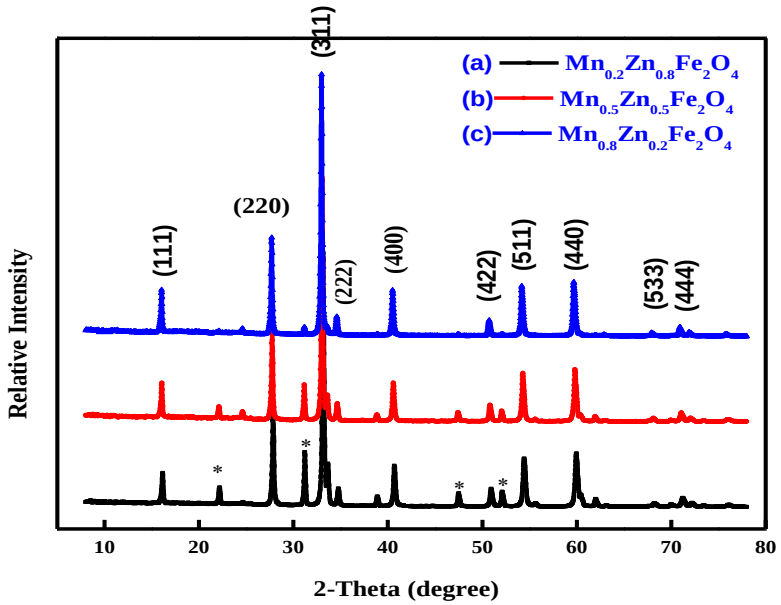

Fig. 2 XRD-diffraction images of (a) $Mn_{0.2}Zn_{0.8}Fe_2O_4$, (b) $Mn_{0.8}Zn_{0.2}Fe_2O_4$, (c) $Mn_{0.5}Zn_{0.5}Fe_2O_4$

It is cleared from SEM micrographs that the samples prepared with co-precipitation technique have the spherical morphology with narrow size distribution. The particle size of the sample was in the range of 50nm to 85nm. It can be seen that lattice parameter increases proportionally to the manganese content 'x' which may be a direct consequence of larger ionic radius of Mn^{+2} (0.91 Å) as compared to Zn^{+2} (0.82 Å) [23]. It has been observed that with the decrease of Zn contents the lattice constant 'a' value is increasing. The values of lattice parameter, crystal density and crystallite size with Zn substitution are shown in table. I.

Table I. Zn substitution 'x', lattice parameter 'a', X-ray density(g/cm3) and crystallite Size D(nm) are given below.

Zn Substitution'x'	Lattice constant 'a'	X-Raydensity (gm/cm^3)	Crystallite Size D(nm)
0	8.72	4.69	85
0.2	8.68	4.74	78
0.4	8.65	4.85	65
0.6	8.58	5.10	58
0.8	8.50	5.14	56
1.0	8.45	5.18	50

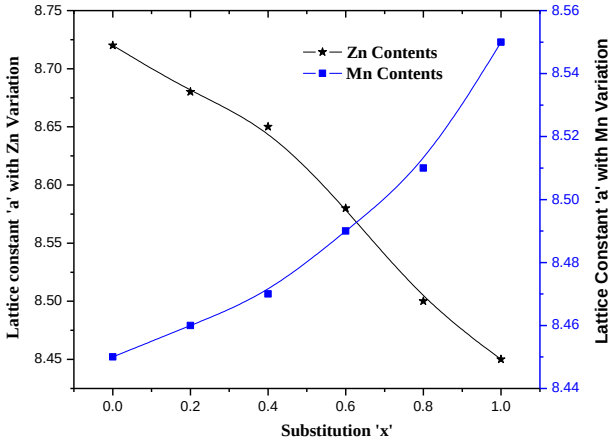

Fig. 3 Variation of Lattice constant 'a' with Mn and Zn contents.

The x-ray density depends on the lattice constant and molecular weight of the sample, where as the mass density (ρ_m) of the samples is being calculated from the geometry and mass of the sample. Both densities ρ_x, ρ_m as a function of Mn concentration are plotted in Fig. 4. It can be seen from the Fig.4 that the X-ray density decreases with the increase of Mn- content x' as it is inversely proportional to the lattice constant, which increases with increasing Mn concentration. Mass density of the ferrite was found to be increasing with x which may be due to the iron reference between Mn and Zn [30] 0r it may be due to the difference in the specific gravity of Mn(7.21g/cm^3) and Zn(7.133g/cm^3), as describe in CRC book[24].

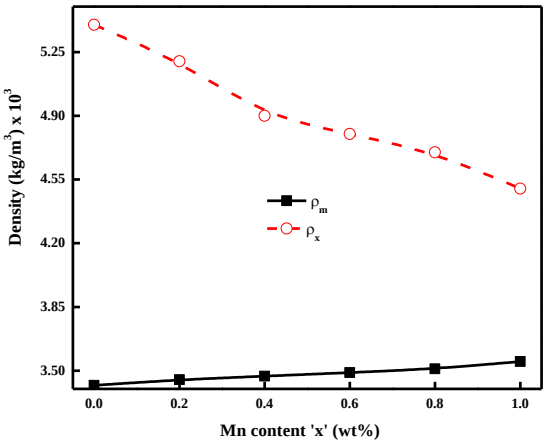

Fig. 4 The variation of X-ray density, sample density with Mn contents.

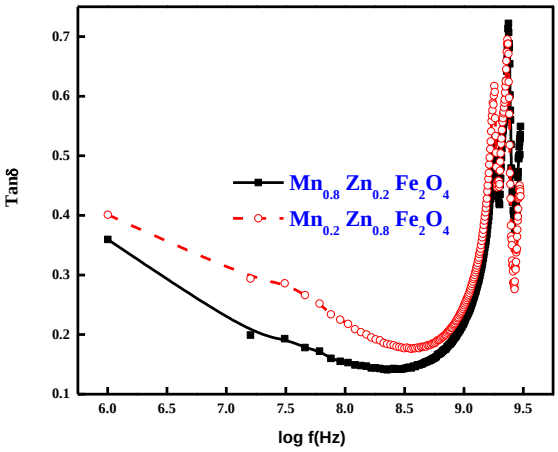

Fig. 5 Tangent loss Vs log f(Hz) (a) $Mn_{0.2}Zn_{0.8}Fe_2O_4$, (b) $Mn_{0.8}Zn_{0.2}Fe_2O_4$,

Figure 5 show the value of dielectric loss at low frequency is high for $Mn_{0.2}Zn_{0.8}Fe_2O_4$ and at high frequency the values remain same or a slight increase in the value of $Mn_{0.8}Zn_{0.2}Fe_2O_4$.

A maximum loss may be observed, when the hopping frequency is nearly equal to that of externally applied electric field. The loss in dielectric arises from the inability of polarization in a molecule to follow the rate of change of the oscillating applied electric field.

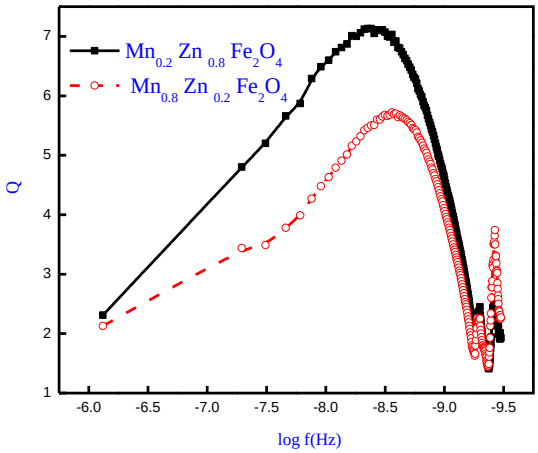

Fig. 6 Quality factor Vs log f (Hz) (a) $Mn_{0.2}Zn_{0.8}Fe_2O_4$, (b) $Mn_{0.8}Zn_{0.2}Fe_2O_4$,

The values of quality factor at low frequency is high for $Mn_{0.2}Zn_{0.8}Fe_2O_4$ but it decreases at high frequency as compare to $Mn_{0.8}Zn_{0.2}Fe_2O_4$ as it is depicted in the Fig. 6. The high Q-values are due to the high resistivity of the samples. The imperfection and defects in $Mn_{0.8}Zn_{0.2}Fe_2O_4$ are lower than $Mn_{0.2}Zn_{0.8}Fe_2O_4$. Smaller grain size is competent for larger quality values. The maximum value of dielectric constant appears at low frequency is the result of interfacial dislocation piles up, grain boundary defect and oxygen vacancies etc. Dielectric constant varies with frequency depicts the dispersion due to Maxwell Wagner interfacial polarization that is in agreement with Koop's phenomenology theory [25-26]. The data shows that the dispersion of the dielectric constant at low frequency comes from the grain boundary and at high frequency it comes from the grains. The value of the real part of dielectric constant decreases with the increase of frequency, the variation of the real part of dielectric constant with frequency is shown in Fig. 7. Electrons are distributed around the nuclei evenly in the absence of an electric field but at the application of electric field; electron cloud is from the nuclei in the direction opposite to the applied field. As a consequence, the separation between the negative and positive charge take

place and the molecule behave like an electric dipole. Three modes of polarization occur that are electronic polarization, atomic polarization and orientation polarization [27].The decrease in dielectric constant with frequency is due to either the lag of dipole oscillations behind those of the applied ac electric field at high frequencies or due to more need of thermal energy to disturb the ordered dipoles at higher frequencies of the applied field [28]. The dielectric material with a heterogeneous structure can be imagined as a structure consists of well conducting grains separated by highly resistive thin layers called grain boundaries. In this case, the applied voltage acts on the small particles (grains) and a space charge polarization is build up at grain boundaries. Space charge polarization is due to the conductivity of the grains and the presence of the free charges at the grain boundary. Koop's proposed that the effect of grain boundaries is predominant at low frequencies. The high value of the dielectric constant is the result of the thinner grain boundaries.The materials which have low dielectric constant are preferred for high frequency applications. The low dielectric constant materials have remarkable penetration depth ability for the electromagnetic waves and these reduce the skin effect [29-32].

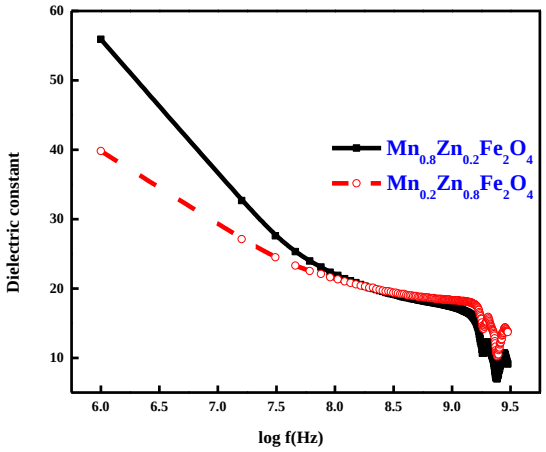

Fig. 7. Dielectric constant Vs log f(Hz) (a) $Mn_{0.2}Zn_{0.8}Fe_2O_4$, (b) $Mn_{0.8}Zn_{0.2}Fe_2O_4$,

The imaginary part of the dielectric constant versus frequency is shown in Fig. 8. The decrease in the imaginary part of dielectric constant with increase in frequency agrees well with the Debye relaxation process. The maximum value in the imaginary part is observed when the hopping frequency is equal to the external electric field frequency. The value of imaginary part of dielectric constant attains a maximum value then it decreases due to the power loss. The dielectric constant is directly proportional to grain size [33, 34].

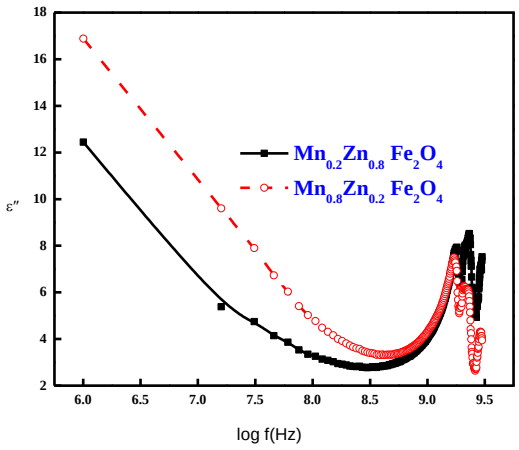

Fig. 8.Imaginary Part of Dielectric constant Vs log f(Hz) (a) $Mn_{0.2}Zn_{0.8}Fe_2O_4$, (b) $Mn_{0.8}Zn_{0.2}Fe_2O_4$.

The value of the imaginary part of dielectric constant is high at the low frequency and vice versa it becomes low at the high frequency $Mn_{0.8}Zn_{0.2}Fe_2O_4$.

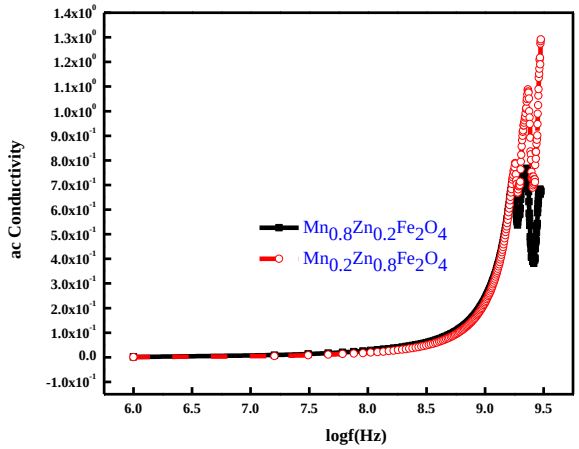

Fig. 9 ac Conductivity Vs log f(Hz) (a) $Mn_{0.2}Zn_{0.8}Fe_2O_4$, (b) $Mn_{0.8}Zn_{0.2}Fe_2O_4$,

The ac conductivity of Mn-Zn ferrites was studied and it was found to be a function of frequency as shown in Fig. 9. The frequency dependent ac conductivity showed a plateau in the low frequency region and dispersion at high frequency region. In the low frequency region the conductivity is independent of frequency and at high frequency, it is frequency dependent. The variation of the ac conductivity with the frequency at room temperature σ_{ac} shows a normal behavior, it increases with the increase of frequency. Frequency dependence of ac conductivity $\sigma(\omega)$ follows the relation [35].

$$\sigma(\omega) = A\omega^n \qquad (5)$$

Where $\omega = 2\pi f$, n is dimensionless exponent and A has the dimensions of $\Omega^{-1}cm^{-1}$ Dielectric constant and ac conduction mechanism are strongly correlated [45].

The variation of resistivity with frequency is shown in Fig.12. At low frequency the resistivity is high, its mean the grain boundary plays an important role but as the frequency becomes high, the resistivity becomes low; so the grains play an effective role at the high frequency and resistivity decreases with the increase of frequency.

The capacitance value is high at low frequencies but it is low at high frequencies as shown in Fig.11. In fact, the alternating voltage half period becomes shorter at high frequencies so the space charge polarization fails to settle itself and capacitance begins to drop. The time required for electronic or ionic polarization to set in is very small as compared with the time of voltage sign change between the two half-period of the applied alternating voltage. The variation of capacitance with frequency is given by the relation [36].

$$C = C_g + [s\tau/(\omega^2\tau^2 + 1)] \qquad (6)$$

Where C_g is geometrical capacitance, s is conductance corresponding to absorption current, τ is the dipole relaxation time and ω is the angular frequency. According to this, capacitance is maximum when $\omega = 0$ and minimum when $\omega = \infty$ [36].

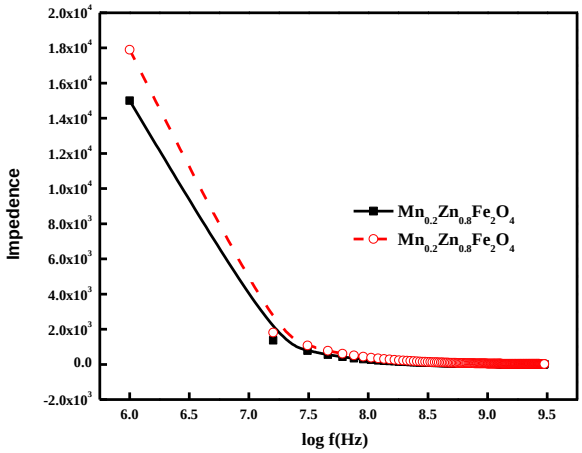

Fig. 10 Capacitance Vs log f (Hz) (a) $Mn_{0.2}Zn_{0.8}Fe_2O_4$, (b) $Mn_{0.8}Zn_{0.2}Fe_2O_4$,

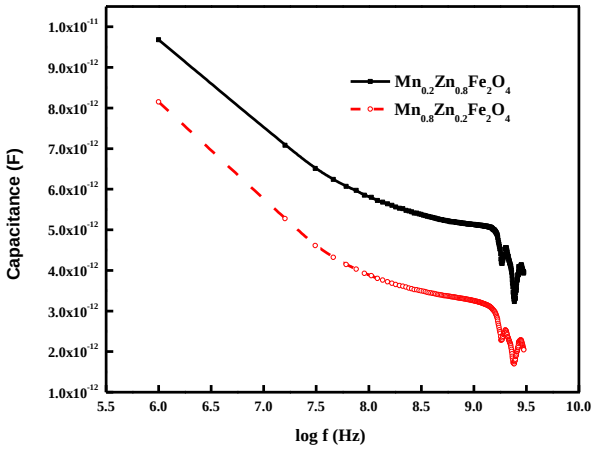

Fig. 11 Capacitance Vs log f (Hz) (a) $Mn_{0.2}Zn_{0.8}Fe_2O_4$, (b) $Mn_{0.8}Zn_{0.2}Fe_2O_4$,

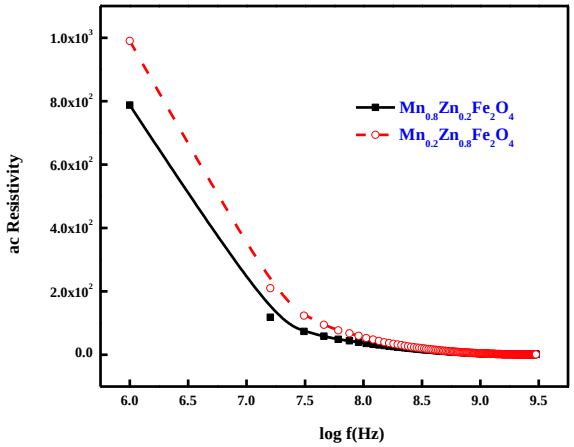

Fig. 12 ac Resistivity Vs log f(Hz) (a) $Mn_{0.2}Zn_{0.8}Fe_2O_4$, (b) $Mn_{0.8}Zn_{0.2}Fe_2O_4$,

The value of ac resistivity of $Mn_{0.8}Zn_{0.2}Fe_2O_4$ is high at low frequency but at high frequency the values of both are almost equal. The resistivity of the ferrite in general depends on several factors such as the density, porosity, grain size, chemical composition etc [37].

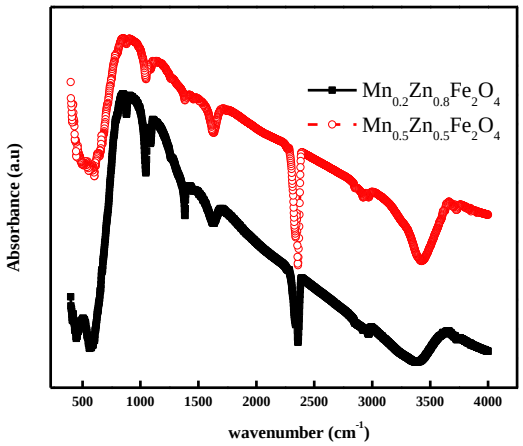

Fig. 13 FTIR spectra of (a) $Mn_{0.2}Zn_{0.8}Fe_2O_4$, (b) $Mn_{0.8}Zn_{0.2}Fe_2O_4$,

FTIR spectroscopy is a very useful technique to deduce the structural investigation and redistribution of cations between octahedral and tetrahedral sites of the spinel structure in Mn-Zn nanoparticles. The band around 1371cm^{-1} is for C-H out of plane deformation vibration. The peak at 2929 cm^{-1} is assigned to methylene (CH_2) group. The adsorbed water is featured by bands at 3416cm^{-1}, 1626cm^{-1}which are assigned to the O-H stretching and H-O-H bonding modes of vibration, respectively. The characteristics peaks of Zn-O stretching vibrations are observed at 2353 cm^{-1}. The presence of band at 1048 cm^{-1} represents the C-O stretching and the band at 593cm^{-1} is attributed to the stretching vibration of tetrahedral and octahedral groups [38-40]. It can be seen from the Fig. 14 that for a given external magnetic field, magnetization of Mn-Zn ferrite powder is clearly related to the substitution degree of Zn. The saturation magnetization decreases with the increase of Zn content because it is non metallic ion. The M-H curves exhibit a linear magnetization with small coercivety indicating that ferrite nanoparticles are super paramagnetic the magnetic domains are based on randomly oriented non-interacting particles [41,42]. The Mn-Zn samples cannot fully saturate at 8KOe, this thing indicates the presence of super paramagnetic and single domain particles. The values of saturation magnetization increased from 4.5emu/g to 18.7 emu/g increases with the increased percentage quantity of manganese contents. The coercivety value for the Nano composite increases from 165 Oe to 272Oe showing increased in magnetization results from Mn contents.

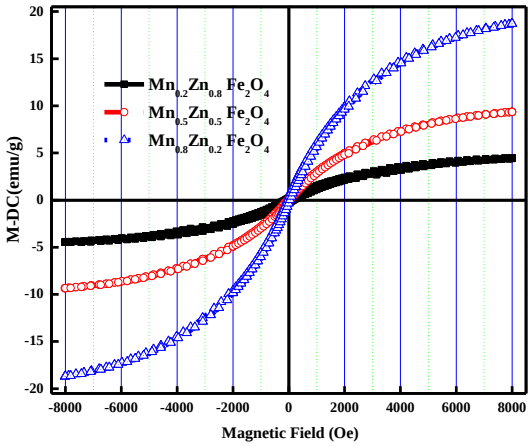

Fig. 12 M-H curves for (a) $Mn_{0.2}Zn_{0.8}Fe_2O_4$ (b) $Mn_{0.5}Zn_{0.5}Fe_2O_4$ (c) $Mn_{0.8}Zn_{0.2}Fe_2O_4$

4. Conclusions

Structural analysis with XRD indicates that the system confirms the formation of Mn-Zn ferrite structure with lattice constant increasing proportionally to the Mn content. The increase in Mn concentration x favours the formation of Mn-Zn ferrites with higher density. X-ray density depends on the lattice constant and molecular weight of the sample shows a decreasing trend with increasing Mn content. Samples of Nano crystalline $Mn_{0.5}Zn_{0.5}Fe_2O_4$ has been successfully synthesized using co-precipitation method. Mn-Zn ferrites exhibit the super paramagnetic behavior so it can be used for electronic devices. The synthesized ferrite sample by the co-precipitation technique exhibits the single phase Face center cubic structure. The crystallite size of the powder varies in the range of 50-85nm and average particle size measured by SEM is 95nm. The increasing value of Zn substitution depicts the crystallite size and lattice parameter decreases while crystal density increases. The saturation magnetization decreases with the increase of non metallic Zn ions while the capacitance increases proportional to Zn contents.

References

[1] H. I. Yoo, H. L. Tuller, J. Phys. Chem. Solids **9(7),**761 (1988).

[2] S. M. abbas, R. Chitterjee, A. K. Dixit, A. V. R. Kumar, T. C. Goel, J. Appl. Phys, **101**, 074105(2007).

[3] R. Che, L. M. Peng, X. Duan, Q. Chen, X. Liang, Adv. Mater, **16,** 401(2004),.

[4]Y.Huang, N. Li, Y. Ma, F. Du, F. Li, X. He, X. Lin, H, Gao, Y. Chen, Carbon **46**, 1614 (2007).

[5] K. H. J. Buschow, Concise Encyclopedia of Magnetic and superconducting Materials, Elsevier Science, (2005).

[6] Siemens Matsushita Components, Ferrites and Accessories, Data Book, **11** (1999).

[7] Vogt Electronic, Inductive components, Ferocarit (Catalogue), **91**,01-22 (2000).

[8] P. M. Botta, P. G. Bercoff, E. F. Aglietti, H. R. Bertorello, J. M. Porto López, Ceramic International, **32(8)** 857 (2006).

[9] M. J. N. Isfahani, M. Myndyk, V. Šepelák, J. Amighian, J. Alloys and Compounds, **470** (1-2) 434 (2009).

[10] Y. Y. Meng, Z. W. Liu, H. C. Dai, H. Y. Yu, D. C. Zeng, S. Shukla, R. V. Ramanujan, Powder Technology, **229**, 270 (2012).

[11] J. G. Hou, Y. F. Qu, W. B. Ma, Q. C. Sun, J. Sol-Gel Sci. and Tech.**44 (1),** 15 (2007).

[12] A. Košak, D. Makovec, M. Drofenik, Material Science Forum, **453,** 219(2004).

[13] T. Nakamura, T. Tsuoka, K. Hatakayama, J. Magn. Magn. Mater, **138,** 319-323(1994).

[14] H. Y. Luo, Z. X. Yue, J. Zhou, J. Magn. Magn.Mater, **210**,104-110 (2000).

[15] H. Shokrollahi, K. Janghorban, Mater. Sci. Eng. B,**141**, 91-107 (2007).

[16] K. T. Mathew, B. S. Kumar, A. Lonappan, J. Jacob, T. Kurien, J. Samuel, T. Xavier, Mater.Chem. Phys. **79,** 187-192 (2003).

[17] T. T. Ahmed, I. Z. Rahman, M. A. Rahman, J. Mater. Process.Tech. **153**, 797 (2004).

[18] P. Hu, H. Yang, D. Pan, H. Wang, J. Tian, S. Zhang, X. Wang, A. A. Volinsky, J. Magn. Magn.Mater.332, (2010).

[19] M. H. Yousefi, S. Manouchehri, A. Arab, M. Mmozaffari, Gh. R. Amiri, J. Amighian, Material Research Bulletin, **45**, 1792-1795 (2010).

[20] E. J. Verwey, F. De. Boer, H. H. Vsanten, J. Chem. Phy., **161**,1091 (1948).

[21] J. D. L. C. P. Bean, J. Appl. Phys., **30,**1205 (1959).

[22] P. Bayliss, D. C. Erd, M. E. More, A. Sabina, D. K. Smith, Mineral Powder Diffraction File, JCPDS, USA, (1986).

[23] T. Abbas,Y. Khan, M. Ahmad, S. Anwar, Solid state commun. **82,** 701 (1992).

[24] D. R. Lide, CRC Handbook of Chemistry and Physics, 76th ed., CRC Press, London, (1995).

[25] J. C. Maxwell, A. Treatise on electricity and Magnetism,. Oxford, NewYork**2**, (1954).

[26] C. G. Koops, Phys. Rev. **83**, 121 (1951).

[27] S. V. Jadhav, V. Puri, Synth.Met.**158**, 883-887 (2008).

[28] S. M. Reda, Dyes Pigments,**75**, 526-532 (2007).
[29] F. Latif, M. Aziz, N. Katun, M. Ali, M. Z. A. Yahya, J. Power Sources. **1594**, 1401 (2006).
[30] S. Havriliak, S. Negami J. Polym. Sci. Part-C. **14**, 99 (1966).
[31] J. C. Maxwell, Electricity and Magnetism, Oxford University Press, London, **1**, (1873).
[32] B. A. Afzal, M. J. Akhtar, M. Nadeem, M. M. Hassan, J. Phys. Chem C, **113**, 17560 (2009).
[33] S. Fang, C. H. Ye, T.Xie, Z. Y. Wong, J. W. Zhao, L. D. Zhang, Appl. Phys. Lett. **88**, 013101 (2006).
[34] Z. Kezhao, Fredkin, R. Donald, J Appl. Phys, **85**, 6187-6192 (1999).
[35] G. Murtaza, I. Ahmad, J. Wu, Mater. Sc. in Semicond.Process.**34**, 269-275 (2015).
[36] E. J. Verwey, F. De.Boer, H. H. Vsanten, J. Chem. Phys, **161,** 1091(1948).
[37] J. D. L. C. P. Bean, J. Appl. Phys. **30,** 1205 (1959).
[38] R. R. Shahraki, M. Ebrahimi, S. A. S. Ebrahimi, S. M. Masoudpanah, J. Magn.Magn. Mater.**324,** 3762-3765 (2012).
[39] H. Soleimani, Z. Abbas, N. Yahya, K. Shameli, H. Soleimani, Int. J. Mol. Sci. **13**, 8540 (2012).
[40] B. S. Kondawar, A. I. Nandapure, B. I. Nandapure, Adv. Mat. Lett.**5(6)**, 339-344 (2014).
[41] G. Murtaza, I. ahmad, A. Hakeem, P. Mao, X. Guohua, M. T. Farid, G. Mustafa, M. Kanwal, M. Hussain, Digest J. Nanomater. Biostructures, **10(4)**, 1393-1401 (2015).
[42] A. Hakeem, G. Murtaza, I. Ahmad, P. Mao, X. Guohua, M. T. Farid, M. Kanwal, G. Mustafa, M. Hussain, M. Ahmad, Digest J. Nanomater. Biostructures, **11(1)**, 149 (2016).